



## Article

# Coastal Wetland Shoreline Change Monitoring: A Comparison of Shorelines from High-Resolution WorldView Satellite Imagery, Aerial Imagery, and Field Surveys

Kathryn E. L. Smith <sup>1,\*</sup> , Joseph F. Terrano <sup>2</sup> , Jonathan L. Pitchford <sup>3</sup> and Michael J. Archer <sup>3</sup>

- <sup>1</sup> U.S. Geological Survey, St. Petersburg Coastal and Marine Science Center, St. Petersburg, FL 33701, USA  
<sup>2</sup> Cherokee Nation System Solutions, U.S. Geological Survey, St. Petersburg Coastal and Marine Science Center, St. Petersburg, FL 33701, USA; [jterrano@contractor.usgs.gov](mailto:jterrano@contractor.usgs.gov)  
<sup>3</sup> Grand Bay National Estuarine Research Reserve, Mississippi Department of Marine Resources, Moss Point, MS 39562, USA; [jonathan.pitchford@dmr.ms.gov](mailto:jonathan.pitchford@dmr.ms.gov) (J.L.P.); [michael.archer@dmr.ms.gov](mailto:michael.archer@dmr.ms.gov) (M.J.A.)  
\* Correspondence: [kelsmith@usgs.gov](mailto:kelsmith@usgs.gov)

**Abstract:** Shoreline change analysis is an important environmental monitoring tool for evaluating coastal exposure to erosion hazards, particularly for vulnerable habitats such as coastal wetlands where habitat loss is problematic world-wide. The increasing availability of high-resolution satellite imagery and emerging developments in analysis techniques support the implementation of these data into shoreline monitoring. Geospatial shoreline data created from a semi-automated methodology using WorldView (WV) satellite data between 2013 and 2020 were compared to contemporaneous field-surveyed Global Position System (GPS) data. WV-derived shorelines were found to have a mean difference of  $2 \pm 0.08$  m of GPS data, but accuracy decreased at high-wave energy shorelines that were unvegetated, bordered by sandy beach or semi-submergent sand bars. Shoreline change rates calculated from WV imagery were comparable to those calculated from GPS surveys and geospatial data derived from aerial remote sensing but tended to overestimate shoreline erosion at highly erosive locations (greater than  $2 \text{ m yr}^{-1}$ ). High-resolution satellite imagery can increase the spatial scale-range of shoreline change monitoring, provide rapid response to estimate impacts of coastal erosion, and reduce cost of labor-intensive practices.

**Keywords:** shoreline change; coastal; wetlands; estuary; satellite imagery; erosion; accretion



**Citation:** Smith, K.E.L.; Terrano, J.F.; Pitchford, J.L.; Archer, M.J. Coastal Wetland Shoreline Change Monitoring: A Comparison of Shorelines from High-Resolution WorldView Satellite Imagery, Aerial Imagery, and Field Surveys. *Remote Sens.* **2021**, *13*, 3030. <https://doi.org/10.3390/rs13153030>

Academic Editor: Jorge Vazquez

Received: 24 June 2021

Accepted: 28 July 2021

Published: 2 August 2021

**Publisher's Note:** MDPI stays neutral with regard to jurisdictional claims in published maps and institutional affiliations.



**Copyright:** © 2021 by the authors. Licensee MDPI, Basel, Switzerland. This article is an open access article distributed under the terms and conditions of the Creative Commons Attribution (CC BY) license (<https://creativecommons.org/licenses/by/4.0/>).

## 1. Introduction

Coastal wetlands serve as a natural barrier between marine and terrestrial habitats and provide essential ecosystem services such as fish and wildlife habitat, carbon sequestration, and natural flood control for upland areas [1,2]. External forcing from sea-level rise, storms, and anthropogenic modifications [3,4] create highly dynamic conditions for coastal wetland evolution, often causing wetland loss through shoreline erosion, interior peat collapse, and submergence. Shoreline erosion is a primary cause of wetland loss in many parts of the world [5] and erosion has been linked to wind-driven waves, sediment availability and delivery, boat traffic, and sea level rise [6–10]. Changes in sea level, sediment delivery, and storm frequency and intensity in coastal areas due to climate and other environmental changes increases the threat of these hazards on wetland survival [11,12]. Environmental monitoring and assessment are critical for detecting the impacts of environmental change and developing adaptive management strategies [11,13]. This is particularly true for coastal areas where erosion hazards are threatening critical habitats such as coastal wetlands.

Shoreline change analysis (SCA) is a common monitoring procedure for evaluating coastline dynamics and the vulnerability of communities and habitats to erosion hazards, such as sea level rise, storms, and anthropogenic modifications [14–16]. SCA involves the

repeated measurement of shoreline position over time and estimating the rate of erosion or accretion based on movement trends over time. The most common method is to calculate the slope of the linear trend of distance against time using ordinary least squares [17]. SCA relies on consistency within two critical elements: identification of the shoreline and how the position is mapped. A shoreline is defined as the boundary between land and water, but because that boundary may be partial or gradual, mapping consistency requires the use of a shoreline proxy [18]. For sandy beach environments, a common practice is to identify the shoreline position based on elevation and a tidal datum, such as mean high water. Other proxies may be the high water line, wet-dry line, cliff base or top, or low water line. For marsh shorelines, many of the water line features are obscured by vegetation, therefore the outer edge of the vegetation is dubbed the “apparent shoreline” [19,20]. As with many shoreline proxies, boundary delineation is influenced by ambiguity and interpretation; however, the water–vegetation boundary can be identified both in the field and from remotely sensed data and, therefore, provides a consistent proxy for wetland shoreline change analyses.

Modern shoreline position is determined from several different types of source data, including field surveys and remote sensing [21]. One of the primary modern sources of shoreline data is laser altimetry, such as Light Detection and Ranging (lidar), where an elevation proxy is identified to delineate the shoreline position [22,23]. Though lidar has been used to map shorelines for coastal wetlands [24], often laser altimeter data are not available or the accuracy is limited for salt marsh shorelines due to poor laser penetration through the dense vegetation [25–27]. Additionally, lidar collection times are irregular or focused on a specific episodic event, such as for post-storm assessment, consequently making it unreliable for regular monitoring of shorelines in coastal wetland habitats. Aerial imagery is another primary source for mapping wetland shoreline position since it is collected semi-regularly (approximately every 2–3 years for most coastal areas in the United States). The disadvantage of aerial imagery is that each image covers a small area and is collected along a flight path, thereby adjacent images may be collected on considerably different days or tidal cycles impacting data consistency [28]. This inconsistency challenges automated procedures to delineate the shoreline position (typically the wet-dry line), making it necessary to manually map the shoreline boundary by digitizing within Geographic Information System (GIS) software and manually correcting for tidal stages [22,29]. Manual digitization of shorelines is costly, time and labor intensive, but continues to be a standard for modern shoreline mapping [29,30].

Advances in remote sensing allow for pixel and object-based classifications of satellite imagery to extract shoreline features and previous studies have used satellite imagery to extract shoreline positions using various methods [31–35], however most of these satellite-based studies focused on beach environments. Maglione et al. [36] developed a method for extracting estuarine shorelines using high-resolution (<2 m spatial resolution) WorldView (WV) imagery (Maxar Technologies, Inc.) but did not evaluate or quantify the accuracy of the delineated shorelines against other available shoreline data. High-resolution satellite imagery could be a valuable source of data for shoreline delineation due to its regular return interval for repeated collection, consistent spectral characteristics, high spatial resolution, and broad-scale coverage. The combination of these factors could make high-resolution satellite imagery more cost effective and efficient for high-frequency environmental monitoring of shoreline change than aerial imagery or lidar.

With the introduction of high-resolution satellite imagery with frequent return intervals, satellite-derived wetland shoreline data could provide the same spatial and temporal detail as other sources of data, including field-based Global Positioning System (GPS) or aerial imagery-derived shoreline data, but gain greater spatial coverage and reduce the cost of shoreline monitoring by either replacing GPS field surveys or reducing the necessity of survey frequency. In this study, we used a semi-automated procedure to map wetland shorelines from WV imagery from 2013 to 2020 and compared them to contemporaneous

shoreline data from GPS and digitized aerial imagery for study sites at the Grand Bay National Estuarine Research Reserve, Moss Point, MS, USA.

## 2. Materials and Methods

### 2.1. Study Area

In 1972, the Coastal Zone Management Act was passed that established the National Estuarine Research Reserve (NERR) system in the United States (US). The NERR system was designed to facilitate long-term research and monitoring, education, and stewardship of estuarine habitats [37]. In 1999, the Grand Bay NERR (GNDNERR), located in the Northern Gulf of Mexico in the state of Mississippi (Figure 1), was designated through a partnership between the National Oceanic and Atmospheric Administration (NOAA) and the Mississippi Department of Marine Resources [38]. The GNDNERR also overlaps portions of the Grand Bay National Wildlife Refuge, located within Alabama and Mississippi. The GNDNERR is approximately 73 km<sup>2</sup> of relatively undisturbed estuarine habitat and contains a variety of habitats such as wet pine savanna, maritime forests, tidal creeks, salt pans, wetlands, bayous, and bays [39]. Grand Bay has diurnal astronomical tides (microtidal with 0.42 m average amplitude) and experiences wind-driven water level fluctuations. The shoreline of Grand Bay is largely vegetated by saltmarsh grasses *Juncus roemerianus* Scheele, *Spartina alterniflora* Loisel., and *Spartina patens* (Aiton) Muhl. with some sandy shorelines along highly dynamic margins.

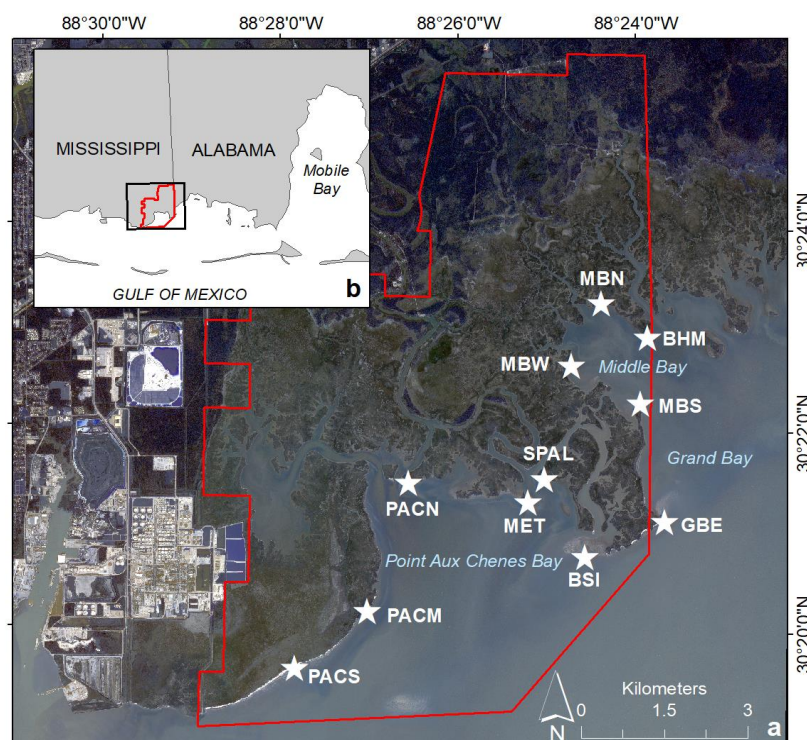


**Figure 1.** Map of the Grand Bay National Estuarine Research Reserve (red boundary line) with white stars depicting the location of shoreline erosion study sites (a). The inset map (b) shows the location of the study region on the border of Mississippi and Alabama, USA, in the northern Gulf of Mexico. Sites names refer to: BHM = Bayou Heron Mouth; MBN, MBW, MBS = Middle Bay North, West, and South, respectively; GBE = Grand Batture East; BSI = Bird Island; SPAL = North Jose Bay; MET = Met Station Island; PACN, PACM, PACS = Point aux Chenes North, Middle, and South, respectively. Data sources: Shoreline from © OpenStreetMap contributors (<https://www.openstreetmap.org/> accessed on 30 October 2018). Image basemap from © Maxar Technologies, 2020 (<https://www.maxar.com/>, accessed on 28 July 2021). All rights reserved.

Wetland loss in the form of shoreline erosion is a pressing management concern at GNDNERR [38,39] and within the northern Gulf of Mexico in general [16,40,41]. Shorelines in some areas of GNDNERR are eroding more than 2 m per year [42]. With a relative sea level rise of 0.41 cm yr<sup>-1</sup> [43], the erosion rates are higher than would be expected based on wetland retreat from sea level rise alone. Exposure to wind-driven waves and reduced sediment supply may all contribute to the high shoreline erosion rates. Wetland shoreline position at various sites within the reserve have been monitored using GPS field surveys on a semi-quarterly basis since 2013 (Figure 1 and Table 1). Sites are generally named after their geographic location, while a few are associated with monitoring stations and include the following: Bayou Heron Mouth (BHM); Middle Bay North, West, and South (MBN, MBW, and MBS, respectively); Grand Batture East (GBE); Bird Island (BSI); North Jose Bay, also known as the *Spartina* Sentinel Site (SPAL); Met Station Island (MET); and Point aux Chenes North, Middle, and South (PACN, PACM, PACS, respectively). The goal of the monitoring program is to understand wetland shoreline dynamics at a finer spatiotemporal scale than could be done with large-scale remote sensing techniques. Due to the labor-intensive nature of field-based surveys, the current study focuses on eleven field sites with different shoreline types and wind-wave exposure and explores a semi-automated technique to map wetland shorelines using WorldView satellite imagery.

**Table 1.** Site location, vegetation, elevation, and sedimentary characteristics for the eleven Grand Bay National Estuarine Research Reserve shoreline erosion study sites.

Site <sup>1</sup>	X Coordinate <sup>2</sup>	Y Coordinate <sup>2</sup>	Species Present <sup>3</sup>	Scarp Height (m)	Marsh Slope	Nearshore Slope	Marsh Elevation (m)	Shoreline Sediment Type <sup>4</sup>
BHM	365771.947	3361950.554	SA, JR	0.26 ± 0.07	0.05 ± 0.02	0.2 ± 0.05	0.25 ± 0.02	M
MBN	364948.644	3362581.497	SA, JR	0.29 ± 0.02	0.04 ± 0.01	0.16 ± 0.01	0.28 ± 0.02	M
MBW	364397.654	3361443.661	SA, JR	0.44 ± 0.03	0.04 ± 0.01	0.13 ± 0.02	0.23 ± 0.02	M
MBS	365652.416	3360740.168	SA	0.32 ± 0.12	0.02 ± 0.01	0.15 ± 0.04	0.36 ± 0.03	M
GBE	366084.354	3358576.051	SA, SP, BF	0.15 ± 0.03	0.08 ± 0.02	0.15 ± 0.06	0.49 ± 0.06	Ss, M
BSI	364642.111	3357926.278	SA, SP	0.15 ± 0.05	0.12 ± 0.03	0.08 ± 0.03	0.46 ± 0.05	Ms, Ss
SPAL	363916.729	3359351.988	SA, JR	0.54 ± 0.04	0.05 ± 0.01	0.11 ± 0.04	0.34 ± 0.02	M
MET	363621.959	3358939.945	SA	0.32 ± 0.04	0.07 ± 0.04	0.17 ± 0.05	0.33 ± 0.02	Ms
PACN	361468.093	3359292.170	SA	0.27 ± 0.02	0.01 ± 0.01	0.25 ± 0.08	0.5 ± 0.01	M
PACM	360722.683	3356944.082	SA, SP	0.16 ± 0.03	0.01 ± 0.01	0.11 ± 0.1	0.49 ± 0.02	M, S
PACS	359405.655	3355908.173	SA	0.18 ± 0.05	0.08 ± 0.02	0.24 ± 0.19	0.46 ± 0.05	S

<sup>1</sup> BHM = Bayou Heron Mouth; MBN, MBW, MBS = Middle Bay North, West, and South, respectively; GBE = Grand Batture East; BSI = Bird Island; SPAL = North Jose Bay; MET = Met Station Island; PACN, PACM, PACS = Point aux Chenes North, Middle, and South, respectively.

<sup>2</sup> Coordinates in the Universal Transverse Mercator Zone 16 North referenced to the North American datum of 1983 (UTM 16N NAD83).

<sup>3</sup> Species codes: SA (*Spartina alterniflora* Loisel), SP (*Spartina patens* [Aiton] Muhl), JR (*Juncus roemerianus* Scheele), BF (*Borrchia frutescens* [L] DC). <sup>4</sup> Sediment codes: M (fine grained/mud), S (sand), Ms (mud with shells or shell hash), Ss (sand with shells or shell hash).

## 2.2. Data

WV-derived shorelines (WVS) were compared to vector digital shoreline data from two other data sources: GPS-based shorelines (GPSS) and aerial imagery-derived shorelines (AIS). Details on data collection and vectorization are included in the following sections for all three shoreline data sets.

### 2.2.1. GPS Data

Since 2013, shoreline positions have been surveyed using real-time kinematic (RTK) GPS at eleven locations in GNDNERR to quantify shoreline change rates. GPS data were collected using a Trimble R8 Model 3 Global Navigation Satellite System (GNSS) and TSC3 data collector from 2013 to 2018, or a Trimble R10 GNSS system and TSC3 data collector from 2018 to 2020. Each were attached onto a 2 m graphite rod with a mounted foot to obtain both horizontal and vertical shoreline position. The positional accuracy of Trimble R8 Model 3 GPS points was ±10 mm + 1 parts per million (ppm) root mean square (RMS) horizontal error and ±20 mm + 1 ppm RMS vertical error [44]. The horizontal error of the Trimble R10 GPS points was ±8 mm + 0.5 ppm RMS and vertical error was ±15 mm + 0.5 ppm RMS [45]. The GPS points were collected roughly 5 to 10 m apart along the vegetation-water boundary, which typically represented the top of an erosional scarp; where an erosional scarp was not visible, the most suitable shoreline position based

on dense shoreline vegetation is mapped. After field data collection, the GPS data were imported into ArcGIS software by Esri [46] as points. Points were connected into lines to create a polyline feature class using the ArcGIS tool Points to Line within the Data Management toolbox for each site and year surveyed.

During May of 2021, additional field RTK GPS and site descriptive data were collected at each site to measure salt marsh platform elevations and estimate platform slope. Between three to five cross-shore transects were selected at each study site depending on the shoreline length (extra transects were collected at sites with longer shorelines). Along each transect, multiple GPS points were surveyed, including two locations in the marsh interior, at the marsh-estuary shoreline (the scarp crest, if present), and two points in the nearshore (one point at the scarp toe, if present). General site descriptions were also noted, including approximate percent cover of vegetation species present at the marsh shoreline using the 1 m quadrat technique [47] and nearshore sediment properties (mud/fine-grained sediments, sand, or presence of shells). These data provided information regarding the cross-shore profile, including the marsh platform elevation and slope, which were used to correct satellite-derived shoreline features for water inundation distance (described in Section 2.2.1. WorldView-derived shoreline accuracy and Equation (3)).

### 2.2.2. Aerial Imagery-Derived Shoreline Data

Orthoimagery from the National Agriculture Imagery Program (NAIP) of the U.S. Department of Agriculture was downloaded via the U.S. Geological Survey (USGS) Earth Explorer (<https://earthexplorer.usgs.gov/>, accessed on 23 February 2021) for available dates between 2013 and 2020. NAIP collected new imagery every 2 to 3 years, with each state following on a cycle. Since GNDNERR is located along the border of two states, parts of the reserve are surveyed more frequently. A total of five NAIP acquisition dates were identified to have coincident spatial and temporal coverage as WV or GPS collection dates for the study sites (Table 2). NAIP imagery has a 1 m ground sample distance with a ground positional accuracy of 5 m. Shoreline position was identified using the land/water boundary as a shoreline proxy for vegetated shorelines or the wet/dry line for whenever beaches were present seaward of the marsh. Shoreline boundaries were digitized at a scale of 1:1,500 from natural color imagery [48].

**Table 2.** The dates of collection for WorldView satellite imagery, Real-time Kinematic Global Positioning System (GPS) field-surveys, and aerial imagery shoreline (AIS) data. The remote sensing data were paired by year with the closest available GPS field survey date.

Year	WorldView Date	GPS Date	NAIP Date
2013	17 December 2013	19 September 2013	
2014	14 November 2014	17 November 2014	15 October 2014
2015	3 May 2015	11 June 2015	
2016	2 July 2016	12 May 2016	24 June 2016
2017	14 May 2017	1 May 2017	
	9 August 2017	14 August 2017	
	30 December 2017	8 November 2017	
2018	23 June 2018	9 May 2018	
		10 December 2018	4 December 2018
2019	16 November 2019	19 June 2019	16 November 2019
2020	17 November 2020	13 November 2020	16 June 2020

### 2.2.3. WorldView-Derived Shoreline Data

High-resolution satellite imagery was obtained for collection dates that overlap the available GPSS and AIS data from either of the two WV satellites with color and infrared spectrum data (WorldView-2 [WV2] or WorldView-3 [WV3] © Maxar Technologies, 2020). Briefly, both WV satellites collect high-spatial resolution imagery (1.84 and 1.24 m, respectively) in eight spectral bands, including five bands for visible wavelengths (coastal blue, blue, yellow, green, and red bands) and three bands for infrared wavelengths (red-edge

and two near-infrared bands). A total of ten dated images between 2013 and 2020 were selected that provided either complete or partially complete coverage of the study area and were collected as close to the date of the GPS field-based shoreline as possible (Table 2). If the closest dated WorldView image had extensive clouds covering the shoreline or minimal study area coverage, the next closest WorldView image date was selected. At least one image was obtained for each year, except for 2017 where three images were selected. The three images in 2017 were collected in May, August, and December and provided additional information on how seasonality might impact automatic shoreline extraction methodology. Images were radiometrically and atmospherically corrected and then pansharpened using ERDAS IMAGINE 2020 (version 16.6.0) to obtain measures of ground reflectance.

To improve comparisons between WVS and AIS, images were automatically co-registered to high-resolution aerial imagery (NAIP) using AutoSync Workstation toolbox in ERDAS Imagine. First, an NAIP image mosaic was created for an extent larger than the WV image coverage. Autosync generates automatic tie points between two images, in this case the WV and NAIP image. The tie points coincident on both images were used to adjust the WV image to the corresponding location on the NAIP. Tie points with an error value greater than 1 m were removed. The co-registration of the WV imagery improved the spatial accuracy of the WV imagery to less than 3.5 m and allowed for the direct comparison of WV and NAIP-derived shoreline data.

To generate vector shorelines from WV images, we modified the methodology described by Maglione et al. [36]. All WV images were classified into binary land-water rasters using tools within ArcGIS. First, normalized difference vegetation index (NDVI) was calculated using WV band 5 in the visible red spectrum (RED) and band 7 in the near infrared spectrum (NIR1) using the following Formula (1):

$$\text{NDVI} = \frac{\text{NIR1} - \text{RED}}{\text{NIR1} + \text{RED}} \quad (1)$$

NDVI is used to estimate the density of vegetation, therefore it distinguishes between vegetation and water or bare soil [49]. Since wetland shorelines in the study area are densely vegetated with salt marsh grasses, the NDVI provided the best approximation of the shoreline position. Maglione et al. [36] provide the following NDVI values for land-water classification: vegetation was classified as high values (above 0.2), water represents low values (usually less than  $-0.2$ ), and soil somewhere in between  $-0.2$  and 0.2. However, the exact threshold used to identify the shoreline may differ depending on the type of wetland, shoreline, and image acquisition parameters. This procedure worked well for vegetated shorelines but was inadequate in areas where sandy or shell beaches were present seaward of the salt marsh, a feature of marsh adjacent to former barrier islands and with high wave energy. Sandy beaches in this region tend to be bright white from high quartz content [50]. To improve the shoreline classification for these beach shorelines, we selected a static threshold (5000) using band 8 (NIR2), which shows high reflectance for the white sand and shell beach. The “beach” classification was merged with the NDVI vegetation layer to create a final binary land-water raster. Several tools within ArcGIS were used to clean raster boundaries and produce a vector shoreline; if not otherwise specified, the default parameters were used. The raster was generalized using Expand and Shrink tools (using 1 cell) to remove any isolated and extraneous pixels, then filtered with Boundary Clean (Spatial Analyst toolbox) to smooth edges. The filtered raster was then converted into polygons (Raster to Polygon tool in Conversion toolbox) and polylines (Polygon to Polyline in the Data Management toolbox). The polylines were smoothed using the Polynomial Approximation with Exponential Kernel (PAEK) algorithm and a 2-m smoothing filter to reduce the cell structured appearance. Sometimes multiple shorelines were identified, including interior marsh ponds or streams, or shorelines were located outside the study area (due to a larger image extent); these extraneous shoreline vectors were manually deleted to produce a clean estuary-marsh shoreline geospatial data set.

### 2.3. Data Analysis

Several analysis techniques were selected to evaluate the accuracy of the WVS to field measurements and determine how well WVS replicated other methods for calculating short-term shoreline change rates. Most of these analyses were conducted in ArcGIS [46] and R [51], utilizing a package called Analyzing Moving Boundaries Using R (AMBUR) [52].

#### 2.3.1. WorldView-Derived Shoreline Accuracy

Since field based GPSS is the most accurate available shoreline position data, we compared the WVS data to GPSS to estimate error in the WVS methodology. Comparisons were made on WVS and GPSS data collected as close together as possible (Table 2). Most comparisons were made on data collected less than two months apart to reduce error associated with time between data collection, such as changes in shoreline position and seasonal tidal cycles. The exception was the 2019 data sets which were approximately five months apart but were the only available data for that year.

Two methods were used to estimate the WVS error based on GPSS measurements. The first was to calculate the distance between the GPSS points and closest WVS vector (the WVS could be either landward or seaward of the GPSS point, thereby always providing a positive value) (Figure 2a). This was performed in ArcGIS using Near Analysis which measures the distance to the closest feature between two data sets. Distances are calculated in meters based on the closest available node on the WVS vector at any angle from the GPS point.

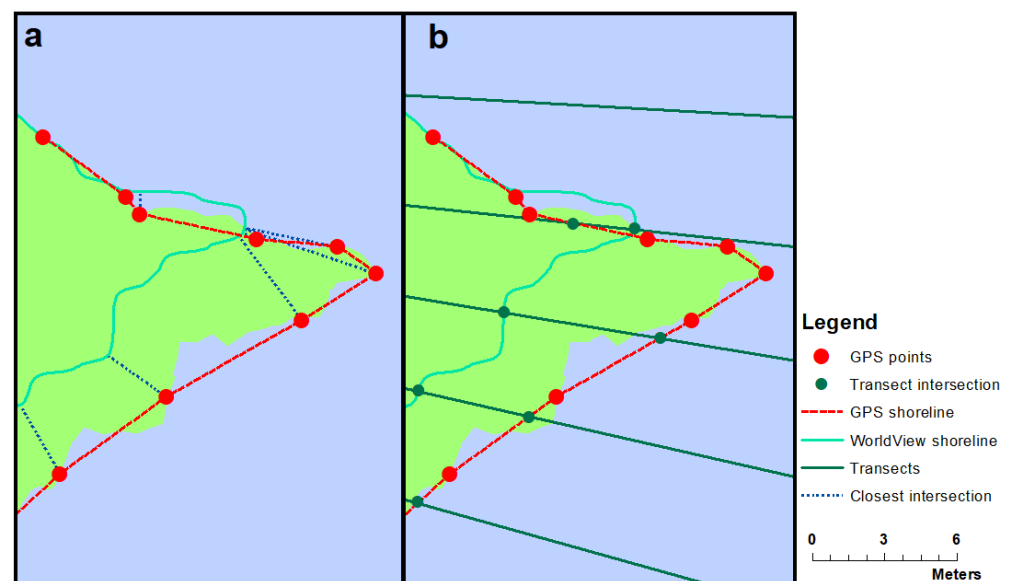


**Figure 2.** Differences between shoreline from WorldView satellite imagery and field-based surveys from Real-time Kinematic Global Positioning System (GPS) are estimated in two ways: (a) the distance between the GPS point and the nearest WV shoreline vector, and (b) the distance between the GPS approximated shoreline (by connecting the points) and the WVS using the intersection along transects.

The second method was to connect the GPSS points to create vector shorelines in ArcGIS, then calculate the distance between the GPSS and WVS along a cross-shore transect (Figure 2b). This calculation was performed using AMBUR [52]. AMBUR is a package within the statistical program R that calculates the distance and rate of change for shorelines using a cross-shore transect-based method. The program generates transects by connecting between offshore and onshore baselines parallel to the shoreline at a set interval distance (for our analyses, we chose 10 m increments between transects). We chose 10 m transect increments to coincide with the spatial resolution of the GPS data, which were collected

approximately 5 to 10 m apart. The program generates points where the transects intersect the shorelines. The distances between the points are calculated to generate shoreline movement distances and rates of change for each transect. Several shoreline change statistics are calculated by AMBUR, but this analysis used the net distance of change ( $\Delta x$ ). The  $\Delta x$  is the distance in meters (m) between the earliest and latest shoreline and provided an estimate of the difference between the GPSS and WVS pairs for each year (the distance between the position along the transect).

Shoreline change rates calculated using only GPSS data were compared with WVS- and AIS-only rates to determine if WVS provided a comparable analysis in to more commonly used remote sensing techniques. Shoreline change rates (also called the linear regression rate or shoreline rate-of-change) were also calculated using AMBUR. The shoreline change rate ( $\hat{b}$ ) is the slope of the best fit line of the linear regression for shoreline distance against calendar date in meters per year ( $\text{m yr}^{-1}$ ). A negative  $\hat{b}$  value indicate erosion, while a positive value indicate accretion. Shoreline change statistics also include a 95% confidence interval (c.i.) used to estimate the confidence in the rate of change statistic. We used the  $\hat{b} \pm \text{c.i.}$  to create shoreline change categories. If both  $\hat{b} + \text{c.i.}$  and  $\hat{b} - \text{c.i.}$  were negative, the shoreline was classified as eroding; if both were positive, the shoreline was classified as accreting; if one was positive and another negative, then the general trend could not be ascertained (uncertainty on whether the shoreline was accreting or eroding) and was therefore classified as stable or indeterminate.

In addition,  $\hat{b}$  from GPSS data ( $\hat{b}_g$ ) were used to correct the  $\Delta x$  estimate for errors due to changes in shoreline position between the GPSS and WVS collection dates. To correct the data, we first used AMBUR to estimate  $\hat{b}_g$  using all available dated GPSS vector data from 2013 to 2020. This provided an average shoreline change rate. The fraction of time between GPSS and WVS date of collection multiplied by  $\hat{b}_g$  provided an estimate of how much that shoreline would have moved between dates. This value was used to adjust the calculated  $\Delta x$  and account for the possible change in shoreline position between sample dates, using the following Formula (2):

$$\Delta x_t = \Delta x + \hat{b}_g * \Delta t \quad (2)$$

where  $\Delta t$  is the time difference between the GPSS and WVS surveys (in fraction of the year) and  $\hat{b}_g$  is the shoreline change rate calculated using GPSS field surveys in AMBUR.

In addition, water level can impact marsh shoreline detection by either obscuring the shoreline (inundating the marsh when water level is high) or confusing detection by exposing nearshore vegetation, such as sparse marsh grasses or seagrass blades. We could find no simple method for correcting shoreline vector position for water level, so we developed the following technique, modified from methods developed for beach environments [53]. If water level was above the marsh platform elevation (determined as the mean of the marsh platform elevation data, data collection described in Section 2.2.1), a simple correction was applied to adjust the horizontal difference between the two shoreline vectors using the following Equation (3):

$$\Delta x_c = \Delta x + \frac{h - m_e}{m_s}, \quad (3)$$

where  $\Delta x_c$  is the tidally corrected difference between GPSS and WVS,  $\Delta x$  is the uncorrected difference,  $h$  is the water level height at the time of image collection,  $m_e$  is the elevation of the marsh platform, and  $m_s$  is the marsh slope. To obtain an estimate of the marsh platform slope ( $m_s$ ), we plotted the field collected GPS elevations against the distance from the shoreline, calculated the linear trend slope (Figure 3). There was a great deal of variability in marsh slope as shown by the low  $R^2$  value (0.26) and the site-based slope calculations that range from 0.01 to 0.12 (Table 1) with a mean of  $0.06 \pm 0.03$ . However, we chose to use 0.07 as a conservative estimate of marsh slope for the study region rather than spatially resolved GPS elevations from each study site to reduce the possibility of over-correcting

the shoreline position for two reasons: (1) marsh tidal flooding has many properties that influence the inundation distance other than slope that would impede water flow which cannot be accounted for, such as surface roughness, sediment type, and vegetation, and (2) if the marsh vegetation canopy is above the water level surface, this procedure could classify it as “land” despite surface inundation based on our method of using NDVI, which detects vegetation.

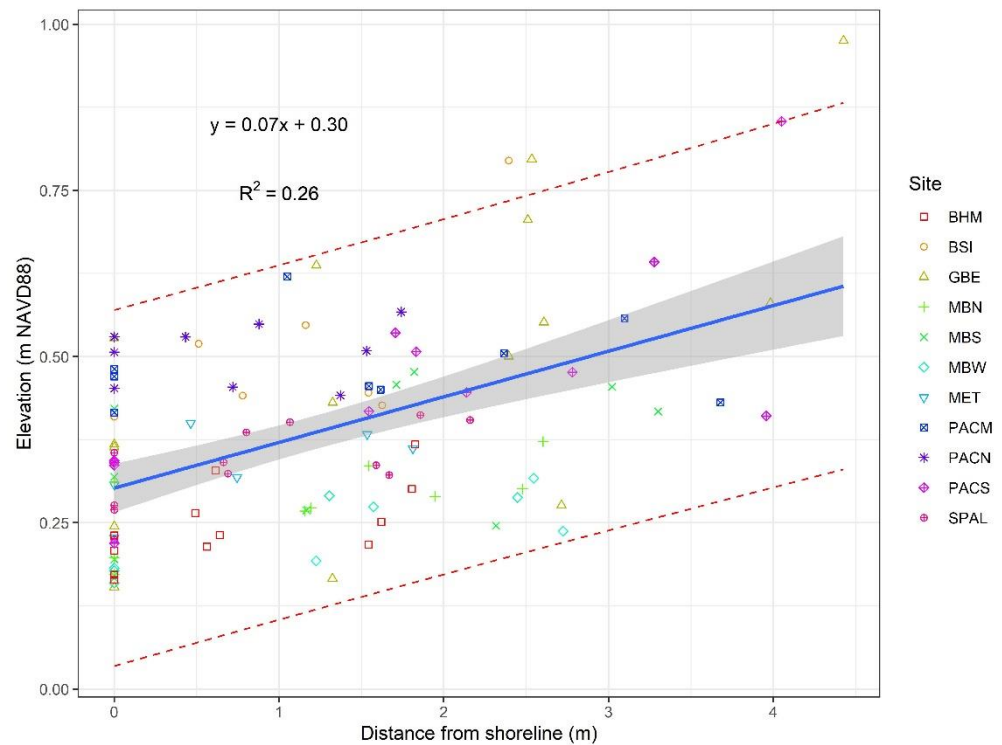


**Figure 3.** Scatter plot of marsh platform elevations against distance from the shoreline (shoreline is located at 0) with the least-squares linear regression line (blue solid line), indicating marsh platform slope is approximately 0.07. Red dashed lines depict the 95% prediction interval and grey-shaded region show the 95% confidence interval. NAVD88 = North American Vertical Datum of 1988. Site names refer to: BHM = Bayou Heron Mouth; MBN, MBW, MBS = Middle Bay North, West, and South, respectively; GBE = Grand Batture East; BSI = Bird Island; SPAL = North Jose Bay; MET = Met Station Island; PACN, PACM, PACS = Point aux Chenes North, Middle, and South, respectively.

The two methods provided different ways of evaluating the accuracy of the WVS in comparison to the best available data (GPSS). The first method provided straightforward differences between field measurements and WVS estimates. The second allowed for temporal adjustments to account for shoreline change between sample dates and examine the impact of water level on WVS estimates. By using two methods (point-based and transect-based) and applying time difference and water level corrections ( $\Delta x_{tc}$ ), we provide a robust evaluation of the WVS methodology in comparison to GPSS data. Data were summarized by calculating the mean  $\pm$  95% c.i. by study site and date for each point or transect (depending on method used).

### 2.3.2. Shoreline Change Comparisons

SCA for WVS was applied to the full study area of GNDNERR using AMBUR. The linear rate of change (LRR) statistic was selected to provide the shoreline rate of change. Cross-shore transects that were located within the eleven shoreline erosion study sites were classified with the study site name. Additionally, SCA from WVS data were compared to rates from the two other methodologies (AIS and GPSS data) to determine whether WVS provided a cost-effective and repeatable methodology for calculating shoreline rates

of change. It is important to note that full WVS were created for each WV image date for the entire GNDNERR study area, whereas the GPSS and AIS were available only for the eleven study sites. This is due to availability, as well as the time- and cost-intensive nature of on-the-ground or manual-digitized shorelines. For these analyses, three sets of shoreline change rates ( $\hat{b}$ ) were calculated using AMBUR (described in Section 2.3.1 WorldView-derived shoreline accuracy) using exclusively WVS ( $\hat{b}_w$ ), GPSS ( $\hat{b}_g$ ), and AIS ( $\hat{b}_a$ ) vector data dated from 2013 to 2020 (2014 to 2020 for AIS data). Shoreline change values using WVS and AIS data sets were compared to GPSS for each transect within the study sites using absolute difference and Bland–Altman plots [54–56]. Bland–Altman plots are a data plotting method that is used to analyze the agreement between two data sets. By comparing  $\hat{b}_w$  and  $\hat{b}_a$  to  $\hat{b}_g$ , we are evaluating whether shorelines derived from the semi-automated method can yield similar results as field data (presumably the most accurate method) and the traditional method of manual digitization of shorelines from aerial imagery.

### 3. Results

The WV-derived shoreline procedure described in the Section 2.2.3 was applied to ten WV images. We visually compared shoreline vectors to the temporally coincident WV imagery displayed as both natural color and color infrared and discovered the value of 0.21 consistently provided an adequate representation of the shoreline (vegetation–water boundary). The accuracy of an automated technique for mapping saltmarsh shoreline position using WV satellite data was quantified by comparing WV-derived shorelines to field-collected GPS shoreline data using both a point- and transect-based technique. Next, we looked at shoreline change rates from all three methods to evaluate whether satellite-based shorelines could be used for future short- and long-term monitoring of wetland shoreline change.

#### 3.1. WVS and GPSS Comparisons

WVS accuracy was estimated by calculating the mean distance between GPSS points collected during a similar time period as the WV image for eleven sites throughout the study area. The mean difference between GPSS points and WVS position was  $2.03 \pm 0.08$  m, but ranged from 0 to 20 m. The mean difference showed large variability between study sites, ranging from  $0.70 \pm 0.06$  to  $4.71 \pm 0.52$  m (Table 3). Sites that were the most accurate in comparison to GPS measurements include SPAL and MBS, both with less than 1 m error between WV and GPS shore position. The shoreline of both these sites have a visible scarp that is vegetated with dense marsh grasses (20–60% estimated percent cover of *Spartina alterniflora*) and nearshore sediments are fine-grained mud. Sites with a difference of greater than 2 m between GPSS and WVS were PACS, BSI, and GBE, all sites with sandy nearshore sediment type. To calculate the mean for the transect-based method, we first took the absolute value in order to accurately account for both negative or positive values (seaward or landward data).

To account for temporal inconsistencies associated with the date of imagery capture, mean distance between GPS point data and WVS were also calculated for each date-paired data set. We evaluated ten image dates, one for each year from 2013 to 2020, with three different data sets in 2017. The mean differences between WVS and GPSS measurements were less variable between years, ranging from 1 to 3 m (Table 4). Water level varied between WV image dates from  $-0.34$  to  $0.54$  m North American Vertical Datum of 1988 (NAVD88) and represented all four seasons. The net difference between GPSS and WVS ranged from  $1.4 \pm 0.18$  to  $3.16 \pm 0.34$  m. The 2014 data had the lowest error with only 4 days between image date and GPS data collection, and water levels below the average marsh platform elevation. The highest error between the WVS and GPSS occurred with the August 2017 image, where the dates between WV and GPS collection were only five days apart, but the image was collected during higher water level ( $0.54$  m NAVD). Overall differences between GPSS and WVS were small, even when uncorrected for water level

variations and temporal differences between image and field data collection dates, well within the image geolocation accuracy (<3.5 m).

**Table 3.** Mean difference between Global Positioning System shorelines (GPSS) and WorldView-derived shorelines (WVS) ( $\Delta x$ ) by study site using both a point and transect-based method. Transect data were corrected for differences between collection date ( $\Delta x_t$ ) and water level ( $\Delta x_{tw}$ ). N is the number of points or transects for each study site.

Site	Points		Transects			
	N	$\Delta x$	N	$\Delta x$	$\Delta x_t$	$\Delta x_{tw}$
BHM	396	1.66 ± 0.15	177	1.79 ± 0.3	1.68 ± 0.3	1.53 ± 0.3
BSI	555	3.82 ± 0.36	278	1.27 ± 0.13	1.18 ± 0.13	0.93 ± 0.11
GBE	777	3.22 ± 0.22	321	5.22 ± 0.59	4.81 ± 0.58	4.75 ± 0.58
MBN	332	1.43 ± 0.11	91	6.69 ± 1.34	6.08 ± 1.39	5.96 ± 1.36
MBS	323	0.93 ± 0.09	99	4.1 ± 0.72	3.9 ± 0.69	3.83 ± 0.68
MBW	311	1.17 ± 0.08	103	6.07 ± 1.28	5.55 ± 1.28	5.46 ± 1.25
MET	529	1.26 ± 0.13	130	1.57 ± 0.43	1.43 ± 0.44	1.38 ± 0.44
PACM	252	1.23 ± 0.19	88	4.08 ± 1.08	4.03 ± 1.08	3.93 ± 1.07
PACN	497	0.92 ± 0.07	122	2.74 ± 0.62	2.65 ± 0.62	2.52 ± 0.6
PACS	264	4.71 ± 0.52	91	0.96 ± 0.13	0.91 ± 0.14	0.72 ± 0.12
SPAL	372	0.7 ± 0.06	137	1.79 ± 0.44	1.63 ± 0.41	1.64 ± 0.41

**Table 4.** Mean difference between Global Positioning System shorelines (GPSS) and WorldView-derived shorelines (WVS) ( $\Delta x$ ) by year using both a point and transect-based method. Transect data were corrected for differences between collection date ( $\Delta x_t$ ) and water level ( $\Delta x_{tw}$ ). N is the number of points or transects for each satellite image date.

Year	Points		Transects			
	N	$\Delta x$	N	$\Delta x$	$\Delta x_t$	$\Delta x_{tw}$
2013	486	2.54 ± 0.26	115	2.83 ± 0.77	2.6 ± 0.76	2.39 ± 0.73
2014	585	1.4 ± 0.18	161	3.85 ± 0.76	3.62 ± 0.75	3.54 ± 0.74
2015	452	1.43 ± 0.11	139	3.17 ± 0.8	2.93 ± 0.79	2.63 ± 0.75
2016	284	1.44 ± 0.22	105	3.21 ± 0.81	3.02 ± 0.8	2.67 ± 0.77
2017	515	2.38 ± 0.28	189	3.58 ± 0.7	3.33 ± 0.69	3.09 ± 0.67
2017	503	3.16 ± 0.34	205	3.08 ± 0.56	2.9 ± 0.55	2.77 ± 0.51
2017	618	1.52 ± 0.15	226	2.75 ± 0.54	2.52 ± 0.53	2.45 ± 0.5
2018	194	1.33 ± 0.23	78	2.46 ± 0.67	2.22 ± 0.62	2.07 ± 0.62
2019	253	2.21 ± 0.21	118	3.48 ± 0.91	3.21 ± 0.89	3.07 ± 0.85
2020	718	2.34 ± 0.24	301	3.18 ± 0.46	2.98 ± 0.45	2.8 ± 0.43

Differences between the GPSS and WVS were higher using the transect-based method compared to the point-based method, even after accounting for time between survey dates and water level, which reduced the difference by 4% to 26%, with the greatest reductions occurring at the sites BSI and PACS. For each date-paired data set, the distance between GPSS and WVS range from  $2.46 \pm 0.67$  to  $3.85 \pm 0.76$  m without water level or temporal corrections; with corrections, the difference between the two data sets decreased, with the highest value for the 2014 data set with  $3.58 \pm 0.75$  m. Temporal and water level corrections accounted for approximately 7% to 13% of the error in the values.

### 3.2. Shoreline Change Analyses

A total of 2422 cross-shore transects were created at an approximate 10 m spacing along the GNDNERR estuarine shoreline. All transects intersect between 4 and 10 WVS with a temporal coverage of 2.5 to 7 years between 2013 to 2020. Using  $\hat{b}_w$  and c.i. to classify shoreline change category, approximately 73.1% of the measured rates indicated shoreline erosion, 25.7% were stable or indeterminate (confidence interval indicates  $\hat{b}_w$  could be either erosional or depositional), and 1.2% of shorelines showed accretion. Mean

shoreline erosion rate was  $-2.46 \pm 0.10 \text{ m yr}^{-1}$  ( $N = 1770$  transects) and mean accretion was  $2.12 \pm 0.48 \text{ m yr}^{-1}$  ( $N = 30$  transects).

Availability of AIS and GPSS limited comparative analyses to transects with all three data sets. A total of 358 transects also contained four or more dated shorelines from each data source. The correlation between  $\hat{b}_w$  and  $\hat{b}_g$  was statistically significant ( $R^2 = 0.89$ ,  $p$ -value  $< 0.001$ ). The correlation plot shows an increase in point spread in the highly erosive measurements and below the trend line, suggesting a slight overestimation of  $\hat{b}_w$  in location with high erosion rates (Figure 4). The correlation between  $\hat{b}_a$  and  $\hat{b}_g$  was also significant ( $R^2 = 0.93$ ,  $p$ -value  $< 0.001$ ). The scatter plot indicates a few values where AIS provided an overestimation of shoreline erosion at low erosive locations.

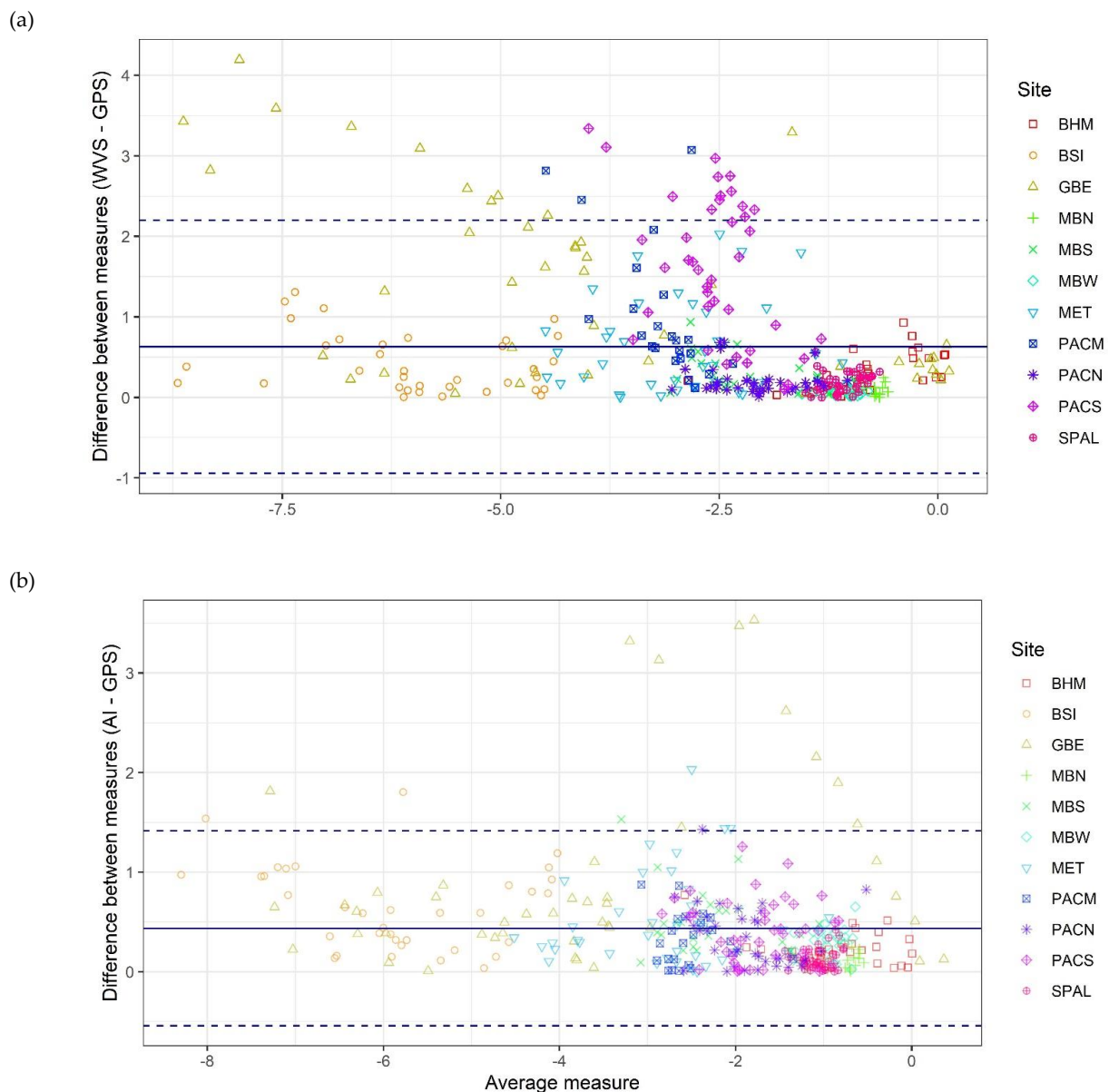


**Figure 4.** Bland–Altman plots showing the rate of shoreline change from Global Positioning System shorelines (GPSS) only versus shoreline change rates calculated from (a) WorldView-derived shorelines (WVS) exclusively and (b) aerial imagery-derived shorelines (AIS) exclusively. Solid blue line depicts the mean and blue dashed lines show the 95% confidence interval.

Mean shoreline change calculated for each site using GPSS, WVS, and AIS data are depicted in Figure 5a. Both  $\hat{b}_a$  and  $\hat{b}_w$  were similar to  $\hat{b}_g$ , with the exception of PACS and PACN sites, where  $\hat{b}_w$  calculated higher erosion rates than the  $\hat{b}_g$ .

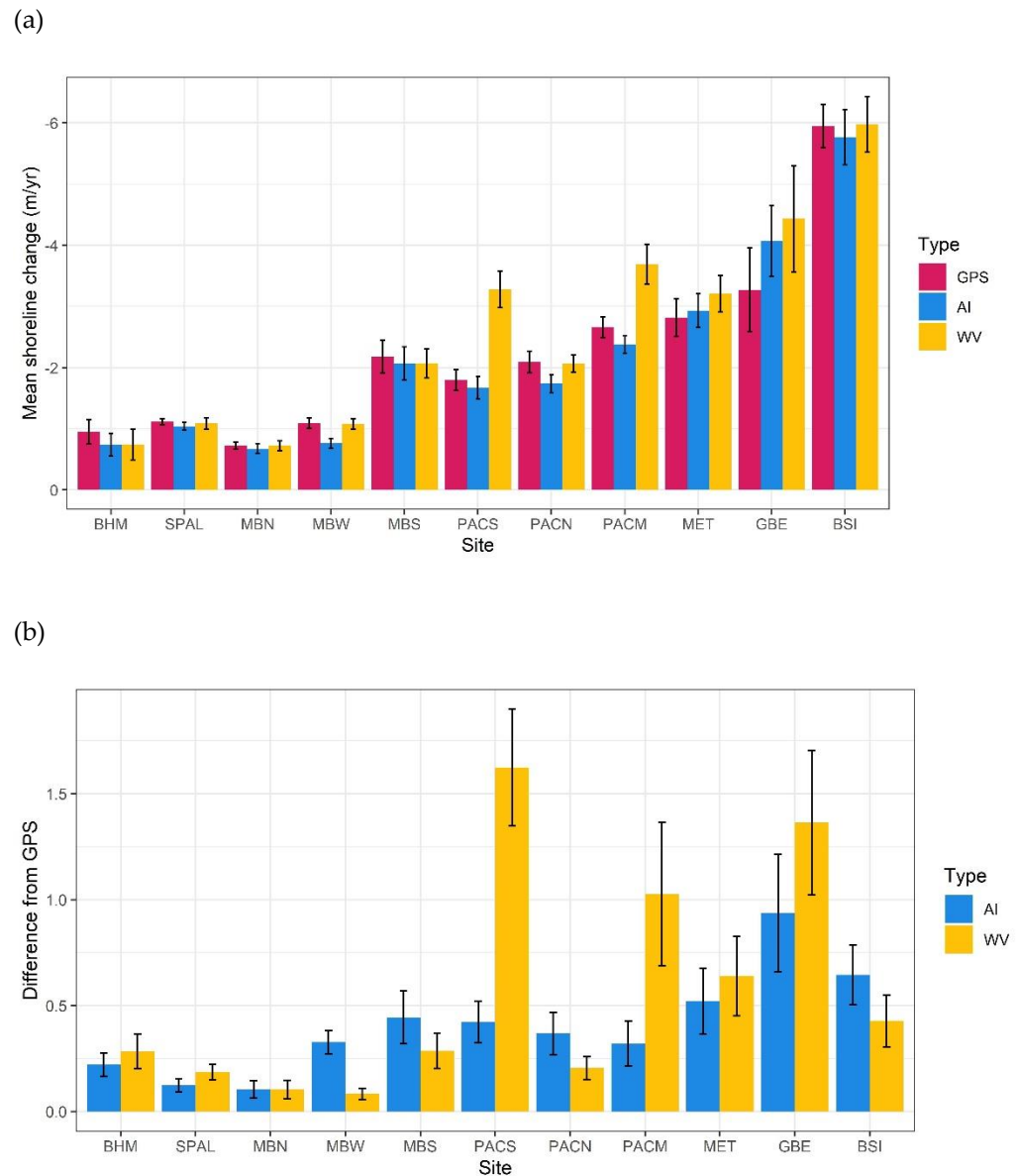


**Figure 5.** Mean shoreline change rate (a) and mean of the absolute difference between the shoreline change rate calculated using Global Position System (GPS) data and shoreline change from two remote sensing data sets: WorldView (WV) satellite imagery and aerial imagery (AI) (b).

The difference between  $\hat{b}_g$  versus  $\hat{b}_w$  and  $\hat{b}_a$  provide an indication of the ability for each shoreline data source to accurately estimate shoreline change calculated from GPSS data (Figure 5b). The mean difference between  $\hat{b}_g$  and  $\hat{b}_w$  was  $0.64 \pm 0.09$  and between  $\hat{b}_g$  and  $\hat{b}_a$  was  $0.44 \pm 0.05$ . The difference between  $\hat{b}_g$  and  $\hat{b}_w$  were lower than  $\hat{b}_a$  at sites MBW, BSI, and PACN, whereas the difference between  $\hat{b}_g$  and  $\hat{b}_a$  were lower than  $\hat{b}_w$  at PACM and PACS.

#### 4. Discussion

Overall difference of the WV-derived shorelines from field-based GPS measurements was low at 2 m and is lower than the geolocation accuracy of the pan-sharpened WV

imagery (approximately 3.5 m). These results support the conclusion that high-resolution satellites provide a valuable data source for monitoring shoreline change of coastal wetland environments. Shorelines with high discrepancies in comparison to field measurements were highly dynamic shorelines exposed to wind-waves from the Gulf of Mexico [57] and high long-term erosion rates [42]. Site characteristics included a gradual slope or indistinct scarp, low (<30%) or no vegetation cover (exposed shoreline), and the presence of shells or sand along the shoreline and in the nearshore (displayed on imagery as white sandy beach). The sand and shells indicate that shoreline would not have been identified using the threshold NDVI technique, rather from the beach threshold analysis step, because the goal of this study was to focus on the vegetated shorelines. Since vegetated estuarine shorelines have been largely overlooked in the literature, a basic approach for sandy shorelines was adopted to include them in this study. The mixed shoreline type (vegetation and beach) is not a unique feature to Grand Bay and can be found frequently in other estuarine and marsh-dominated coastlines; therefore, a methodology that adopts a mixed analysis approach to address multiple shorelines types would be more appropriate for regional or national estuarine shoreline mapping programs. The simple method used here can be improved in light of other research that use high-resolution imagery (WV and other satellite data) to delineate beach shorelines [22,31,53], which may provide a method to improve delineations of wetland shorelines that are bordered by sandy beach. In addition, we discovered an NDVI value of 0.21 consistently provided an adequate representation of the shoreline (vegetation-water boundary) for coastal marsh habitat of southern Mississippi. This value may not provide an adequate boundary when applied to other wetland habitat types, such as mangrove or salt marsh where *Juncus* or *Spartina* are not the dominant species and should be investigated further.

The transect-based method resulted in higher differences than the point-base comparisons between the field-based data and satellite shorelines. This could be due to several and possibly compounding reasons. First, the transect-based method requires the GPSS points to be converted to a line, therefore the shoreline in between each GPS point is not a “true” shoreline. This results in the transect measuring the difference between an approximation of the shoreline from GPS data (based on adjacent measurements) and the satellite-derived shoreline. This approximation could introduce error depending on the distance between points and shoreline sinuosity. Second, the transect-based analysis method is well-documented and used by many researchers for shoreline change analyses but was developed for sandy ocean-facing shorelines [14,17,30,58–63]; estuarine and wetland shorelines are generally more sinuous and spatially complex than ocean-facing beach shorelines. Because the shorelines frequently curve and bend, transects that extend from a baseline at regular intervals toward the shore may intersect the shoreline at an obtuse or acute angle rather than directly perpendicular to the shoreline (example can be noted on Figure 2 of a small-scale spit feature). When transects intersect shorelines at angles greater or less than 90°, distances between shoreline vectors are impacted and therefore the rates change. Techniques to reduce this effect are to increase transect frequency or creating curvilinear baselines that closely match the bends of the shoreline, however both options would require a greater time investment for data analyses. Other methodologies for evaluating shoreline changes over time, such as point-based techniques that evaluate distances between shoreline points [59,64], “fuzzy boundaries” techniques [65], Bayesian methods [15], or machine learning [66,67] may be appropriate for the gradual, indistinct boundaries common to wetland and estuarine shorelines. Calkoen et al. [68] evaluated machine learning techniques against ordinary least squares regression techniques (the transect-based approach explored here) to predict future shoreline change, but research that evaluates different shoreline extraction methods and their impact on statistical calculation of shoreline change rates for estuarine shorelines is a topic that warrants greater attention.

When corrected for shoreline change rate and water level, the difference between GPSS and WVS decrease, indicating that survey date and water level have an impact on the position of satellite-derived shorelines. Therefore, field verification data should be

collected as close as possible to the date of satellite image collection with the maximum interval dependent on shoreline change rates. The maximum interval between field and image collection date would be less of a concern for slowly changing coastlines, whereas would have a greater impact on rapidly changing (eroding or accreting) shorelines. This process could explain the discrepancies between WVS and GPSS, particularly with high erosion rates. Shoreline position was not adjusted to water level prior to rate of change analyses and therefore the higher rates of change may be a product of changing water level conditions. Other studies applied water level corrections to satellite-derived beach shorelines [31,53], but we could not find examples where similar corrections were applied to vegetated shorelines. Other variables, such as vegetation and soil characteristics, could impact both sensor detection of shoreline position and distance of inundation, therefore we used a conservative estimate of marsh slope to avoid over-correction and provide our analysis to demonstrate the need to consider these impacts on results. There was a great deal of variability in marsh slope as shown by the low  $R^2$  value and the site-based slope calculations that range from 0.01 to 0.12, highlighting the potential importance of this variable in evaluating water level impacts on the detection of shoreline position. To our knowledge, this is the first attempt to correct shoreline position for marsh inundation from high water level at the time of image collection and the method requires refinement. Methods could be improved with greater attention to characteristics of wetland inundation and the interpretation of vegetated shoreline position by optical sensors. Additionally, methods that have been shown to improve wetland classifications from Landsat might be adopted to improve overall results of wetland shoreline features [69]. Another option is to select imagery of consistent water level or tidal datum to reduce variability caused by water level. Given the high revisit time of many high-resolution satellites (approximately once per day for WV2 and WV3), the availability of cloud-free imagery of appropriate water levels could be substantial. Considering the timing and environmental conditions during image collection when using high-resolution satellite imagery to delineate vegetated shorelines is important since tidal flooding and vegetation can impact shoreline position.

## 5. Conclusions

One of the greatest challenges to environmental monitoring is access to timely and consistent data that can be efficiently analyzed to support both short- and long-term management decision-making, restoration planning, and resiliency studies. Coastal wetlands have not received as much attention as ocean-facing sandy beaches for broad-scale shoreline change assessments, but wetlands are critically important resources to protect coastal communities from storms, provide habitat and refugia for economically important fish and shellfish species, act as water purifiers for floodwaters, and store carbon within organic rich sediments. In many areas of the United States and the world, availability of modern high-resolution wetland shorelines is non-existent, or data are out-of-date due to data limitations or the labor-intensive process for mapping these areas. The availability of high-resolution satellite imagery and new developments in rapid image analysis techniques can help fill the data gap and provide critical information for coastal wetland monitoring programs. Primary conclusions from this research include:

- A simple procedure to auto-delineate wetland shorelines from WorldView imagery was performed and, compared with field-survey data, resulted in an accuracy of approximately 2 m, but ranged from 0 to 20 m. Shorelines with gradual nearshore slope and sparse shoreline vegetation (bare mud or beach) may reduce boundary distinction and introduce positional error.
- Shoreline change analyses calculated exclusively from wetland shorelines extracted from WorldView imagery were strongly correlated to shoreline change calculations from field-based data ( $R^2 = 0.89$ ,  $p$ -value  $< 0.001$ ) indicating that these satellite-derived shorelines can provide an adequate assessment of short-term shoreline change by extending the applicability of field-based surveys to much larger areas. The timing of image collection and water level are important considerations when selecting imagery.

Further characterization of the impact of these considerations on wetland shoreline position could improve future analyses and methodology.

- Improvement of the auto-delineation of mixed shoreline types (wetland, sandy beaches, rocky cliffs, etc.) that are common in estuaries or evaluate the effectiveness of the transect-based shoreline change analyses and other methodologies on wetland and estuarine shorelines is possible, particularly using other methodologies, such as fuzzy boundaries or pixel-based analyses, may have greater success for gradual or indistinct boundaries commonly found in coastal wetlands and estuaries.
- Shorelines derived from high-resolution (meter-scale spatial resolution) satellite data with superior spatiotemporal coverage can provide a valuable data source to managers for frequent (e.g., annually) and consistent broad-scale monitoring of coastal wetlands or after extreme erosion events.

**Author Contributions:** Conceptualization, K.E.L.S.; methodology, K.E.L.S., J.F.T., J.L.P., and M.J.A.; field data collection, J.L.P. and M.J.A.; geospatial analysis, J.F.T. and K.E.L.S.; formal analysis, K.E.L.S. and J.F.T.; investigation, K.E.L.S.; resources, K.E.L.S.; data curation, J.F.T. and J.L.P.; writing—original draft preparation, K.E.L.S. and J.F.T.; writing—review and editing, K.E.L.S., J.F.T., J.L.P., and M.J.A. All authors have read and agreed to the published version of the manuscript.

**Funding:** The geospatial and statistical analyses for this manuscript was supported by program funds from the United States Geological Survey Coastal and Marine Hazards and Resources Program. Field work was supported by an award from the Office for Coastal Management, National Ocean Service, National Oceanic and Atmospheric Administration and the Mississippi Tidelands Trust Program administered by the Mississippi Department of Marine Resources.

**Data Availability Statement:** Data are available in the following publication: Terrano, J.F.; Smith, K.E.L.; Pitchford, J.P.; Archer, M.J. Shorelines from high-resolution WorldView satellite imagery, Real-time kinematic global positioning data, and aerial imagery for 2013 to 2020 for study sites within Grand Bay National Estuarine Research Reserve, Mississippi. U.S. Geological Survey Data Release, 2021, doi: 10.5066/P9W8TNQM. Worldview-2 and Worldview-3 imagery were provided by the Commercial Data Purchases (CDP) Imagery and archived at the USGS Earth Resources Observation & Science Center (EROS), doi:10.5066/P9VBGMOU.

**Acknowledgments:** The authors would like to acknowledge the staff of the Grand Bay Estuarine Research Reserve for field support and monitoring efforts. The content of this manuscript was greatly improved through the peer review comments from Zafer Defne (USGS), Julie Bernier (USGS), and two anonymous reviewers.

**Conflicts of Interest:** The authors declare no conflict of interest.

**Disclaimer:** Any use of trade, firm, or product names is for descriptive purpose only and does not imply endorsement by the U.S. Government.

## References

1. Chmura, G.L.; Anisfeld, S.C.; Cahoon, D.R.; Lynch, J.C. Global carbon sequestration in tidal, saline wetland soils. *Glob. Biogeochem. Cycles* **2003**, *17*, 1111. [\[CrossRef\]](#)
2. Ennis, B.; Peterson, M.S.; Strange, T.P. Modeling of inundation characteristics of a microtidal saltmarsh, Grand Bay National Estuarine Research Reserve, Mississippi. *J. Coast. Res.* **2014**, *30*, 635–646. [\[CrossRef\]](#)
3. Morris, J.T.; Sundareshwar, P.V.; Nietch, C.T.; Kjerfve, B.; Cahoon, D.R. Responses of coastal wetlands to rising sea level. *Ecology* **2002**, *83*, 2869–2877. [\[CrossRef\]](#)
4. Ravens, T.M.; Thomas, R.C.; Roberts, K.A.; Santschi, P.H. Causes of salt marsh erosion in Galveston Bay, Texas. *J. Coast. Res.* **2009**, *2009*, 265–272. [\[CrossRef\]](#)
5. Marani, M.; d’Alpaos, A.; Lanzoni, S.; Santalucia, M. Understanding and predicting wave erosion of marsh edges. *Geophys. Res. Lett.* **2011**, *38*, L21401. [\[CrossRef\]](#)
6. Kirwan, M.L.; Guntenspergen, G.R. Influence of tidal range on the stability of coastal marshland. *J. Geophys. Res.* **2010**, *115*, F02009. [\[CrossRef\]](#)
7. Leonardi, N.; Ganju, N.K.; Fagherazzi, S. A linear relationship between wave power and erosion determines salt-marsh resilience to violent storms and hurricanes. *Proc. Natl. Acad. Sci. USA* **2016**, *113*, 64–68. [\[CrossRef\]](#)

8. Bilkovic, D.M.; Mitchell, M.M.; Davis, J.; Herman, J.; Andrews, E.; King, A.; Mason, P.; Tahvildari, N.; Davis, J.; Dixon, R.L. Defining boat wake impacts on shoreline stability toward management and policy solutions. *Ocean. Coast. Manag.* **2019**, *182*, 104945. [[CrossRef](#)]
9. Stevenson, J.C.; Ward, L.G.; Kearney, M.S. Vertical accretion in marshes with varying rates of sea level rise. In *Estuarine Variability*; Wolfe, D.A., Ed.; Academic Press: Cambridge, MA, USA, 1986; pp. 241–259.
10. Leonardi, N.; Fagherazzi, S. How waves shape salt marshes. *Geology* **2014**, *42*, 887–890. [[CrossRef](#)]
11. Day, J.W.; Christian, R.R.; Boesch, D.M.; Yáñez-Arancibia, A.; Morris, J.; Twilley, R.R.; Naylor, L.; Schaffner, L.; Stevenson, C. Consequences of climate change on the ecogeomorphology of coastal wetlands. *Estuaries Coasts* **2008**, *31*, 477–491. [[CrossRef](#)]
12. Scavia, D.; Field, J.C.; Boesch, D.F.; Buddemeier, R.W.; Burkett, V.; Cayan, D.R.; Fogarty, M.; Harwell, M.A.; Howarth, R.W.; Mason, C.; et al. Climate change impacts on US coastal and marine ecosystems. *Estuaries* **2002**, *25*, 149–164. [[CrossRef](#)]
13. Wigand, C.; Ardito, T.; Chaffee, C.; Ferguson, W.; Paton, S.; Raposa, K.; Vandemoer, C.; Watson, E. A climate change adaptation strategy for management of coastal marsh systems. *Estuaries Coasts* **2017**, *40*, 682–693. [[CrossRef](#)]
14. Dolan, R.; Michael, S.F.; Stuart, J.H. Temporal analysis of shoreline recession and accretion. *J. Coast. Res.* **1991**, *7*, 723–744.
15. Plant, N.G.; Robert Thieler, E.; Passeri, D.L. Coupling centennial-scale shoreline change to sea-level rise and coastal morphology in the Gulf of Mexico using a Bayesian network. *Earth's Future* **2016**, *4*, 143–158. [[CrossRef](#)]
16. Pendleton, E.A.; Barras, J.A.; Williams, S.J.; Twichell, D.C. *Coastal Vulnerability Assessment of the Northern Gulf of Mexico to Sea-Level Rise and Coastal Change*; USGS: Reston, VA, USA, 2010; p. 26.
17. Thieler, E.R.; Danforth, W.W. Historical shoreline mapping (II): Application of the digital shoreline mapping and analysis systems (DSMS/DSAS) to shoreline change mapping in Puerto Rico. *J. Coast. Res.* **1994**, *10*, 600–620.
18. Boak, E.H.; Turner, I.L. Shoreline definition and detection: A review. *J. Coast. Res.* **2005**, *21*, 688–703. [[CrossRef](#)]
19. Shalowitz, A.L. *Shore and Sea Boundaries: With Special Reference to the Interpretation and Use of Coast. and Geodetic Survey Data*; US Department of Commerce: Washington, DC, USA, 1964; Volume 2.
20. Ellis, M.Y. *Coastal Mapping Handbook*; US Government Printing Office: Washington, DC, USA, 1978.
21. Parrish, C.E. Shoreline mapping. In *Advances in Mapping from Remote Sensor Imagery: Techniques and Applications*; Yang, X., Li, J., Eds.; CRC Press: Boca Raton, FL, USA, 2013; pp. 145–168.
22. Liu, H. Shoreline mapping and coastal change studies using remote sensing imagery and LIDAR data. In *Remote Sensing and Geospatial Technologies for Coastal Ecosystem Assessment and Management*; Springer: Berlin/Heidelberg, Germany, 2009; pp. 297–322.
23. Stockdon, H.F.; Sallenger, A.H., Jr.; List, J.H.; Holman, R.A. Estimation of shoreline position and change using airborne topographic Lidar data. *J. Coast. Res.* **2002**, *18*, 502–513.
24. Farris, A.S.; Defne, Z.; Ganju, N.K. Identifying salt marsh shorelines from remotely sensed elevation data and imagery. *Remote Sens.* **2019**, *11*, 1795. [[CrossRef](#)]
25. Hladik, C.; Alber, M. Accuracy assessment and correction of a LIDAR-derived salt marsh digital elevation model. *Remote Sens. Environ.* **2012**, *121*, 224–235. [[CrossRef](#)]
26. Montané, J.M.; Torres, R. Accuracy assessment of lidar saltmarsh topographic data using RTK GPS. *Photogramm. Eng. Remote Sens.* **2006**, *72*, 961–967. [[CrossRef](#)]
27. Schmid, K.A.; Hadley, B.C.; Wijekoon, N. Vertical accuracy and use of topographic LIDAR data in coastal marshes. *J. Coast. Res.* **2011**, *27*, 116–132. [[CrossRef](#)]
28. Maxwell, A.E.; Warner, T.A.; Vanderbilt, B.C.; Ramezan, C.A. Land cover classification and feature extraction from National Agriculture Imagery Program (NAIP) Orthoimagery: A review. *Photogramm. Eng. Remote Sens.* **2017**, *83*, 737–747. [[CrossRef](#)]
29. Moore, L.J. Shoreline mapping techniques. *J. Coast. Res.* **2000**, *16*, 111–124.
30. Burningham, H.; Fernandez-Nunez, M. Shoreline change analysis. In *Sandy Beach Morphodynamics*; Elsevier: Amsterdam, The Netherlands, 2020; pp. 439–460.
31. Chen, W.-W.; Chang, H.-K. Estimation of shoreline position and change from satellite images considering tidal variation. *Estuar. Coast. Shelf Sci.* **2009**, *84*, 54–60. [[CrossRef](#)]
32. Kuleli, T.; Guneroglu, A.; Karsli, F.; Dihkan, M. Automatic detection of shoreline change on coastal Ramsar wetlands of Turkey. *Ocean. Eng.* **2011**, *38*, 1141–1149. [[CrossRef](#)]
33. Toure, S.; Diop, O.; Kpalma, K.; Maiga, A.S. Shoreline detection using optical remote sensing: A review. *ISPRS Int. J. Geo-Inf.* **2019**, *8*, 75. [[CrossRef](#)]
34. Minghelli, A.; Spagnoli, J.; Lei, M.; Chami, M.; Charmasson, S. Shoreline extraction from WorldView2 satellite data in the presence of foam pixels using multispectral classification method. *Remote Sens.* **2020**, *12*, 2664. [[CrossRef](#)]
35. García-Rubio, G.; Huntley, D.; Russell, P. Evaluating shoreline identification using optical satellite images. *Mar. Geol.* **2015**, *359*, 96–105. [[CrossRef](#)]
36. Maglione, P.; Parente, C.; Vallario, A. Coastline extraction using high resolution WorldView-2 satellite imagery. *Eur. J. Remote Sens.* **2014**, *47*, 685–699. [[CrossRef](#)]
37. Mills, K.; Kennish, M.J.; Moore, K.A. Research and monitoring components of the National Estuarine Research Reserve System. *J. Coast. Res.* **2008**, 1–8. [[CrossRef](#)]
38. Grand Bay National Estuarine Research Reserve. *Grand Bay National Estuarine Research Reserve Management Plan. 2013–2018*; Grand Bay National Estuarine Research Reserve, Mississippi Department of Marine Resources: Moss Point, MI, USA, 2013; p. 104.

39. Peterson, M.S.; Waggy, G.L.; Woodrey, M.S. *Grand Bay National Estuarine Research Reserve: An Ecological Characterization*; Grand Bay National Estuarine Research Reserve: Jackson, MI, USA, 2007; p. 280.
40. Walker, H.J.; Coleman, J.M.; Roberts, H.H.; Tye, R.S. Wetland Loss in Louisiana. *Geogr. Ann.* **1987**, *69*, 189–200. [[CrossRef](#)]
41. Ragoonwala, A.; Jones, C.E.; Ramsey Iii, E. Wetland shoreline recession in the Mississippi River Delta from petroleum oiling and cyclonic storms. *Geophys. Res. Lett.* **2016**, *43*, 11–652. [[CrossRef](#)]
42. Terrano, J. *An Evaluation of Marsh Shoreline Erosion and Sediment Deposition in the Grand Bay National Estuarine Research Reserve, Mississippi, USA*; University of South Florida: Tampa, FL, USA, 2018.
43. National Oceanic and Atmospheric Administration. NOAA Tides and Currents Sea Level Trends: Dauphin Island, AL—Station ID: 8735180. Available online: [https://tidesandcurrents.noaa.gov/sltrends/sltrends\\_station.shtml?id=8735180](https://tidesandcurrents.noaa.gov/sltrends/sltrends_station.shtml?id=8735180) (accessed on 9 May 2021).
44. Trimble. Trimble R8 GNSS Receiver Datasheet. Available online: <http://www.inlandgps.com/Products/R8M3%20Datasheet%20200911.pdf> (accessed on 16 February 2021).
45. Trimble. Trimble R10 GNSS Receiver Datasheet. Available online: [https://geospatial.trimble.com/sites/geospatial.trimble.com/files/2019-04/022516-332A\\_TrimbleR10-2\\_DS\\_USL\\_0419\\_LR.pdf](https://geospatial.trimble.com/sites/geospatial.trimble.com/files/2019-04/022516-332A_TrimbleR10-2_DS_USL_0419_LR.pdf) (accessed on 16 February 2021).
46. Esri Inc. *ArcGIS Desktop*; Version 10.7.1; Esri Inc.: Redlands, CA, USA, 2019.
47. Bonham, C.D. *Measurements for Terrestrial Vegetation*; John Wiley & Sons: Hoboken, NJ, USA, 2013.
48. Terrano, J.F.; Smith, K.E.L.; Pitchford, J.P.; Archer, M.J.; Brochard, M. *Shorelines from High-Resolution WorldView Satellite Imagery, Real-Time Kinematic Global Positioning Data, and Aerial Imagery for 2013 to 2020 for Study Sites within Grand Bay National Estuarine Research Reserve, Mississippi*; Grand Bay National Estuarine Research Reserve: Jackson, MI, USA, 2021.
49. McFeeters, S.K. The use of the Normalized Difference Water Index (NDWI) in the delineation of open water features. *Int. J. Remote Sens.* **1996**, *17*, 1425–1432. [[CrossRef](#)]
50. Mehring, J.L.; McBride, E.F. Origin of modern quartzarenite beach sands in a temperate climate, Florida and Alabama, USA. *Sediment. Geol.* **2007**, *201*, 432–445. [[CrossRef](#)]
51. R Core Team. *R: A Language and Environment for Statistical Computing*; Version 4.0.5; R Foundation for Statistical Computing: Vienna, Austria, 2021.
52. Jackson, C.W., Jr. *AMBUR Package for R Basic User Guide (Windows)*; R-Forge: Savannah, GA, USA, 2010.
53. Vos, K.; Harley, M.D.; Splinter, K.D.; Walker, A.; Turner, I.L. Beach slopes from satellite-derived shorelines. *Geophys. Res. Lett.* **2020**, *47*, e2020GL088365. [[CrossRef](#)]
54. Bland, J.M.; Altman, D.G. Statistical methods for assessing agreement between two methods of clinical measurement. *Int. J. Nurs. Stud.* **2010**, *47*, 931–936. [[CrossRef](#)]
55. Bangdiwala, S.I.; Shankar, V. The agreement chart. *BMC Med. Res. Methodol.* **2013**, *13*, 97. [[CrossRef](#)]
56. Altman, D.G.; Bland, J.M. Measurement in medicine: The analysis of method comparison studies. *J. R. Stat. Soc.* **1983**, *32*, 307–317. [[CrossRef](#)]
57. Nowacki, D.J.; Ganju, N.K. Sediment dynamics of a divergent bay-marsh complex. *Estuaries Coasts* **2020**, *44*, 1216–1230. [[CrossRef](#)]
58. Byrnes, M.R.; McBride, R.A.; Penland, S.; Hiland, M.W.; Westphal, K.A. Historical changes in shoreline position along the Mississippi sound barrier islands. In *Proceedings of the Coastal Depositional Systems in the Gulf of Mexico: Quaternary Framework and Environmental Issues—Twelfth Annual Research Conference, Gulf Coast Section, SEPM, Houston, TX, USA, 8–11 December 1991*; pp. 43–55.
59. Cowart, L.; Walsh, J.; Corbett, D.R. Analyzing estuarine shoreline change: A case study of Cedar Island, North Carolina. *J. Coast. Res.* **2010**, *26*, 817–830. [[CrossRef](#)]
60. Leatherman, S.P. Shoreline Change Mapping and Management Along the U.S. East Coast. *J. Coast. Res.* **2003**, *38*, 5–13.
61. Miller, T.L.; Morton, R.A.; Sallenger, A.H., Jr.; Moore, L.J. *National Assessment of Shoreline Change; A GIS Compilation of Vector Shorelines and Associated Shoreline Change Data for the U.S. Gulf of Mexico*; Open-File Report 2004-1089; U.S. Geological Survey: Reston, VA, USA, 2004.
62. Morton, R.A.; Miller, T.; Moore, L. Historical shoreline changes along the US Gulf of Mexico: A summary of recent shoreline comparisons and analyses. *J. Coast. Res.* **2005**, *21*, 704–709. [[CrossRef](#)]
63. Thieler, E.R.; Hammar-Klose, E.S. *National Assessment of Coastal Vulnerability to Sea-Level Rise: Preliminary Results for the U.S. Gulf of Mexico Coast*; Open-File Report 00-179; U.S. Geological Survey: Woods Hole, MA, USA, 2000.
64. Price, F.D. *Quantification, Analysis, and Management of Intracoastal Waterway Channel Margin Erosion in the Guana Tolomato Matanzas National Estuarine Research Reserve, Florida*; Florida State University: Tallahassee, FL, USA, 2005.
65. Wang, F.; Hall, G.B. Fuzzy representation of geographical boundaries in GIS. *Int. J. Geogr. Inf. Syst.* **1996**, *10*, 573–590. [[CrossRef](#)]
66. Choung, Y.-J.; Jo, M.-H. Comparison between a Machine-Learning-Based Method and a Water-Index-Based Method for Shoreline Mapping Using a High-Resolution Satellite Image Acquired in Hwado Island, South Korea. *J. Sens.* **2017**, *2017*, 8245204. [[CrossRef](#)]
67. Manaf, S.A.; Mustapha, N.; Sulaiman, M.N.; Husin, N.A.; Hamid, M.R.A. Artificial Neural Networks for Satellite Image Classification of Shoreline Extraction for Land and Water Classes of the North West Coast of Peninsular Malaysia. *Adv. Sci. Lett.* **2018**, *24*, 1382–1387. [[CrossRef](#)]

- 
68. Calkoen, F.; Lujendijk, A.; Rivero, C.R.; Kras, E.; Baart, F. Traditional vs. machine-learning methods for forecasting sandy shoreline evolution using historic satellite-derived shorelines. *Remote Sens.* **2021**, *13*, 934. [[CrossRef](#)]
  69. Allen, Y.C.; Couvillion, B.R.; Barras, J.A. Using multitemporal remote sensing imagery and inundation measures to improve land change estimates in coastal wetlands. *Estuaries Coasts* **2012**, *35*, 190–200. [[CrossRef](#)]